Journal of Nuclear Materials 377 (2008) 359–369

Contents lists available at ScienceDirect

Journal of Nuclear Materials

journal homepage: www.elsevier.com/locate/jnucmat

Oxidation kinetics and oxygen diffusion in low-tin Zircaloy-4 up to 1523 K

X. Ma, C. Toffolon-Masclet *, T. Guilbert, D. Hamon, J.C. Brachet

CEA-Saclay, Nuclear Materials Department, SRMA/LA2M, F-91191 Gif-Sur-Yvette, France

ARTICLE INFO

Article history:
Received 15 December 2006
Accepted 5 March 2008

PACS:
81.65.Mq
82.20.Wt
82.56.Lz

ABSTRACT

This paper deals with the study of oxidation kinetics and the identification of oxygen diffusion coefficients of low-tin Zy-4 alloy at intermediate (973 K $\leqslant T \leqslant$ 1123 K) and high temperatures ($T \geqslant$ 1373 K). Two different cases were considered: dissolution of a pre-existing oxide layer in the temperature range 973 K $\leqslant T \leqslant$ 1123 K and oxidation at $T \geqslant$ 1373 K. The results are the following ones: in the temperature range 973–1123 K, the oxygen diffusion coefficient in α_{Zr} phase can be expressed as $D_\alpha = 6.798 \exp(-217.99\ \text{kJ/RT})\ \text{cm}^2/\text{s}$. In the temperature range 1373–1523 K, the oxygen diffusion coefficients in α_{Zr}, β_{Zr} and ZrO_2, were determined using an 'inverse identification method' from experimental high temperature oxidation data (i.e., ZrO_2, and $\alpha_{Zr}(O)$ layer thickness measurements); they can be expressed as follows: $D_\alpha = 1.543 \exp(-201.55\ \text{kJ/ RT})\ \text{cm}^2/\text{s}$, $D_\beta = 0.0068 \exp(-102.62\ \text{kJ/ RT})\ \text{cm}^2/\text{s}$ and $D_{ZrO_2} = 0.115\exp(-143.64\text{kJ/RT})\text{cm}^2/\text{s}$. Finally an oxygen diffusion coefficient in α_{Zr} in the temperature range 973 K $\leqslant T \leqslant$ 1523 K was determined, by combining the whole set of results: $D_\alpha = 4.604\exp(-214.44\ \text{kJ/RT})\ \text{cm}^2/\text{s}$. In order to check these calculated diffusion coefficients, oxygen concentration profiles were determined by Electron Probe MicroAnalysis (EPMA) in pre-oxidized low-tin Zy4 alloys annealed under vacuum at three different temperatures 973, 1073 and 1123 K for different times, and compared to the calculated profiles. At last, in the framework of this study, it appeared also necessary to reassess the Zr–O binary phase diagram in order to take into account the existence of a composition range in the two zirconia phases, α_{ZrO_2} and β_{ZrO_2}.

1. Introduction

During some hypothetical Pressurized Water Reactor (PWR) accidental scenarii such as Loss Of Coolant Accident (LOCA), the nuclear fuel claddings are subjected to a high temperature oxidation (from the LOCA embrittlement criteria point of view, the oxidation temperatures range up to ~1473 K) caused by the interaction of the steam with the metallic cladding material. This leads to the growth of brittle phases, such as $\alpha_{Zr(O)}$ and ZrO_2, from the parent (ductile) β_{Zr} phase. This phenomenon has been mainly studied experimentally; but, in modern fuel cladding alloys, there is still a need for a better quantification and modelisation of the related phenomena. Thus it appeared useful to develop a computational tool able to predict the evolution of the microstructure of low-tin Zy-4 during high temperature oxidation and also at intermediate oxidation temperatures. Then, this approach can be applied to other modern Zr base alloys.

During the past few years, CEA (Commissariat à l'Energie Atomique) has been involved in the development of computer tools able to forecast metallurgical and thermal-mechanical behaviour of Zr alloys under normal and accidental conditions. Particularly, a thermodynamic and a kinetic databases, respectively named 'Zircobase' [1] and 'Zircomob' [2], have been developed using THERMOCALC© and DICTRA© softwares [3]. These tools allow to perform calculations both in equilibrium conditions (prediction of phase equilibria, thermodynamic properties...) and metastable conditions (phase transformations controlled by diffusion...). One of the objective of this work was to re-assess oxygen diffusion coefficients in the α_{Zr} and the β_{Zr} phases in low-tin Zy-4, using recent experimental data.

In a first part, we present the theory of the analytical models used at low and high temperatures (respectively $T \leqslant$ 1123 K and $T \geqslant$ 1273 K). Then, in a second part, the results of some recent experiments performed in order to obtain refined data necessary to apply the analytical model, are presented. In a third part, the oxygen diffusion coefficients in ZrO_2, α_{Zr} and β_{Zr} of low-tin Zy-4 are derived. Then, oxygen concentration profiles were calculated at different times and temperatures and compared to experimental data (i.e. oxygen diffusion profiles).

2. Materials and experiments

The experimental samples were taken from as-received industrial cladding tubes of low-tin Zy-4 from AREVA-NP. The typical chemical composition of the alloy is presented in Table 1.

* Corresponding author. Tel.: +33 16908 2139; fax: +33 16908 7130.
E-mail address: caroline.toffolon@cea.fr (C. Toffolon-Masclet).

0022-3115/$ - see front matter © 2008 Elsevier B.V. All rights reserved.
doi:10.1016/j.jnucmat.2008.03.012

Table 1
Typical chemical composition of low-tin Zy-4 alloys (wt%)

Sn	Fe	Cr	O	Zr
1.3	0.2	0.1	0.13	Bal.

Some of the samples were previously subjected to steam oxidation at 688 K during 549 days for sample A and 240 days for sample B. Table 2 gives the resultant average oxide thickness obtained. The thickness was measured on optical micrographs. Due to the low oxidation temperature used, there was no significant diffusion of oxygen within the suboxide metallic α_{Zr} layer. It was checked using EPMA; at this spatial resolution, no preferential oxygen diffusion along the α_{Zr} grain boundaries was observed (Fig. 1).

Then in a second step, the samples have been heat-treated in a two-level ultrahigh-vacuum chamber at three different temperatures, 973 K, 1073 K and 1123 K for different times which are reported in Table 7. The base pressure in the chamber (4×10^{-5} Torr) was achieved by using liquid nitrogen trapped diffusion. The samples were cooled down in air.

After the heat treatment, the samples were cut to prepare a cross section and then polished. The residual oxide film thickness was measured again at different locations on the tube, using optical microscope, equipped with analySIS® software. It was supposed that no adsorption of oxygen occurred during the heat treatment. The thickness values are given in Table 7.

Finally, the oxygen concentration profiles in the sub-oxide α_{Zr} phase were measured using Electron Probe MicroAnalysis (CAMECA – SX100).

Remark: Due to the steam oxidation process at 688 K, there is a significant hydrogen pick-up ($\sim$ a few hundred weight-ppm) in the samples. However, in this paper, the potential hydrogen influence on the oxygen diffusion coefficient in the α_{Zr} phase has been ignored (for the limited amount of hydrogen considered here).

3. Theory and modelling

Pawel [4] calculated the oxygen diffusivity in α_{Zr} and zirconia phases of Zy-4 in the temperature range 1273–1773 K, by introducing the tracer diffusivity of oxygen in β_{Zr} phase of Zy-4, which was measured by Perkins [5]. Rosa and Haget [6] got oxygen diffusivity in hypostoichiometric zirconia in the temperature range of 1048–1323 K, using oxygen diffusivity in α_{Zr} and β_{Zr} phases. Meanwhile, Debuigne [7] studied the oxygen diffusion in pure zirconium and got the oxygen diffusivity in α_{Zr}, β_{Zr} and zirconia phases.

More recently, Brachet et al. [8] obtained some experimental data on phase growth and oxygen diffusion profiles in low-tin Zy-4 alloy in the temperature range 1373–1523 K. This allowed us to use an inverse identification method [7] to calculate oxygen diffusivities in the phases of low-tin Zy-4 at high temperature and improve the related data in zirconium kinetic database Zircomob04 [2] (version 2004 of Zircomob).

The method applied by Debuigne [7] is used for a system which can be treated as semi-infinite. In this model, the diffusion coefficient is independent of the oxygen concentration. Roy [9] shows that interstitial type atom diffusion, like oxygen in zirconium alloys, takes place in the nearly rigid metal atom lattice by the motion of interstitial atoms at much faster rates than the motion of the substitutional metallic atoms. Therefore, in this paper the calculated chemical diffusivity is taken to be equivalent to the intrinsic diffusion coefficient of the oxygen.

Table 2
Initial thickness of ZrO_2 measured on samples A and B

	$l_{\phi,0}$, μm
Sample A	22.6 ± 3.2
Sample B	16.8 ± 2.8

In Debuigne's thesis [7], the oxygen concentration $C(x;t)$ in the phases are expressed as follows:

$$C(x;t) = A + B\mathrm{erf}\left(\frac{x}{2\sqrt{Dt}}\right). \tag{1}$$

where C is the amount of oxygen, in g/cm^3; erf is the error function; x is the diffusion length, in cm; t is time, in s; and D is the oxygen diffusion coefficient, in cm^2/s. The boundary and initial conditions relevant to this system allows the constants A and B to be evaluated for diffusion within each phase.

3.1. Determination of oxygen diffusivity at low-temperatures ($T \leqslant 1123$ K)

The highest limit of the phase domain considered in this section, 1123 K, is higher than the $\alpha/\alpha + \beta$ transition in Zy-4 alloys that is 1083 K. Indeed we consider that in the temperature range 1083 to 1123 K, that is in the low $\alpha + \beta$ phase domain, the overall O volume diffusion coefficient is nearly equivalent to an alloy containing 100% α_{Zr} and that the influence of the β phase can be neglected considering that, at this temperature, the β phase fraction is very low (<20%), the O solubility limit in α_{Zr} is highly superior to the one in β_{Zr} and O diffusion is much higher in α_{Zr} than in β_{Zr}.

At temperatures below the $\alpha/\alpha + \beta$ transition (1083 K), the dissolution of a pre-existing zirconia layer is illustrated in Fig. 2. Here ϕ is the zirconia phase, $C_{\phi/\alpha}$ is the equilibrium oxygen concentration in zirconia at the α/ϕ interface, in g/cm^3, and $C_{\alpha/\phi}$ is the equilibrium oxygen concentration in α_{Zr} at the α/ϕ interface, in g/cm^3. Within short times, α_{Zr} phase side can be treated as semi-infinite.

The boundary and initial conditions used in the calculation can be expressed by Eq. (2):

$$\begin{cases} C_\alpha = C_{\alpha/\phi} & \text{for} \quad x = 0, t > 0 \\ C_\alpha = C_\alpha(\infty) & \text{for} \quad x > 0, t = 0. \end{cases} \tag{2}$$

Here we assume that $C_\alpha(\infty)$ is equal to the initial oxygen concentration in as-received low-tin Zy-4, C_0, namely $C_\alpha(\infty) = C_0 \approx$ 0.13 wt% $\approx$ 8.5E-3 g/cm^3. This initial condition supposes that no oxygen diffusion occurs during the steam oxidation at 688 K, which has been validated by EPMA analyses (see Section 2).

So the oxygen concentration in α_{Zr}, C_α, can be expressed as

$$C_\alpha = C_{\alpha/\phi} - (C_{\alpha/\phi} - C_0)\mathrm{erf}\left(\frac{x}{2\sqrt{D_\alpha t}}\right). \tag{3}$$

From the Fick's first law, the oxygen flux value in the bulk is

$$-D_\alpha \mathrm{d}C/\mathrm{d}x = (C_{\alpha/\phi} - C_0)\sqrt{\frac{D_\alpha}{\pi t}}\exp\left(-\frac{x^2}{4D_\alpha t}\right). \tag{4}$$

So the amount of oxygen dissolved from the zirconia into the metal, $M(t)$ in mol/cm^2, is given by

$$M(t) = 2\frac{1}{MO}(C_{\alpha/\phi} - C_0)\sqrt{\frac{D_\alpha t}{\pi}}. \tag{5}$$

Using the thickness of the zirconia layer, the density of the oxide, 5.82 g/cm^3 [8], and the ZrO_2 molar mass M_{ZrO_2}, 123.22 g mol^{-1}, the amount of oxygen in the zirconia per unit surface area (=2 times number of oxidized Zr atoms) can be calculated and then the amount of oxygen dissolved from the zirconia into the bulk can be deduced by the variation of the thickness of the zirconia layer after each heat treatment.

Low-tin Zy-4 is a low-alloyed material. So for the α/ϕ interface, oxygen concentration, $C_{\alpha/\phi}$, can be calculated from the Zr–O binary phase diagram.

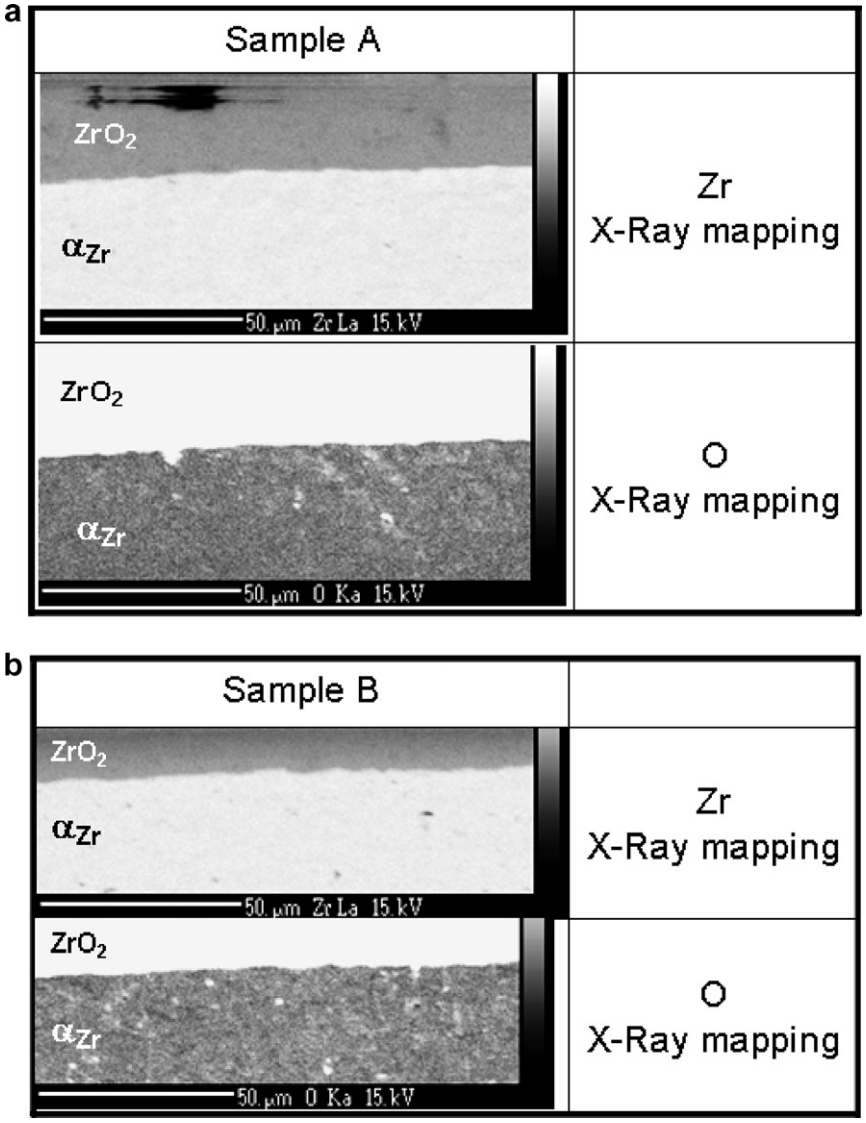

Fig. 1. Zr and O X-Ray mapping obtained by EPMA on Samples A and B after steam oxidation at 688 K.

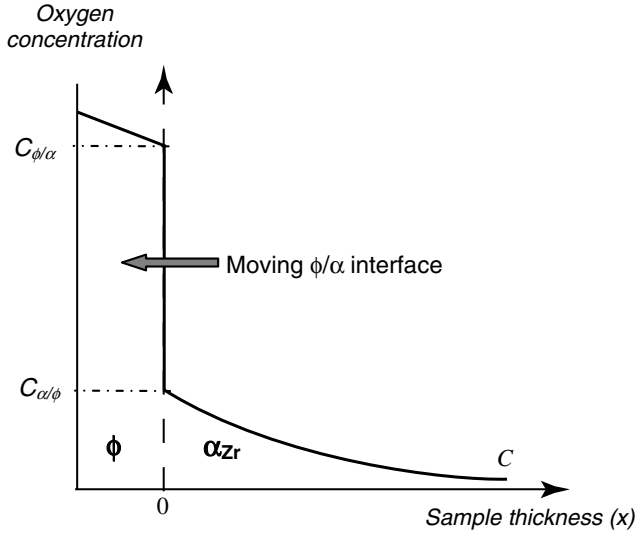

Fig. 2. Schematic diagram representing the dissolution of a pre-existing zirconia layer at temperatures below the α/β transition.

The diffusion coefficient can then be obtained from the plot of M versus $t^{0.5}$.

3.2. Determination of oxygen diffusivity at high temperature ($T \geqslant 1273$ K)

At temperatures above the α/β transition, there are three phases: zirconia and two terminal solution metallic phases, α_{Zr} and β_{Zr}. Fig. 3 is the schematic representation of low-tin Zy-4 oxidized at temperature above the α/β transition.

In Fig. 3, $x = 0$ denotes the initial position of the metal surface. The other parameters are

x_1: distance from the ϕ/α interface to the initial position of the metal surface, in cm;
x_2: distance from the β/α interface to the initial position of the metal surface, in cm;
l_ϕ: thickness of the ϕ phase, in cm;
l_α: thickness of the α phase, in cm;
$C_\alpha(0)$: 'virtual' α_{Zr} oxygen concentration at $x = 0$, in g/cm^3;
$C_\beta(0)$: 'virtual' β_{Zr} oxygen concentration at $x = 0$, in g/cm^3;

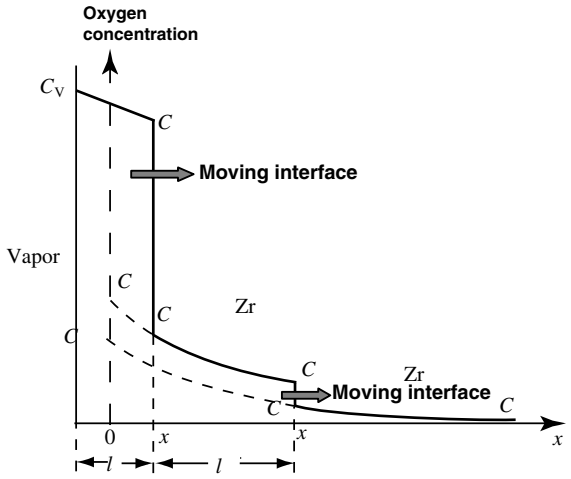

Fig. 3. Schematic diagram of Zy-4 oxidized at temperature above the α/β transition temperature.

$C_{\phi/V}$: equilibrium oxygen concentration in zirconia at the vapor/ϕ interface, in g/cm^3;
$C_{\alpha/\beta}$: equilibrium oxygen concentration in α_{Zr} at the α/β interface, in g/cm^3;
$C_{\beta/\alpha}$: equilibrium oxygen concentration in β_{Zr} at the α/β interface, in g/cm^3.

In this part, we try to identify oxygen diffusion coefficient in zirconia, α_{Zr} and β_{Zr} phases from the experimental results [8]. Within the limited time of the experiments, we treated β_{Zr} phase side as infinite. The initial and boundary conditions used in this work are similar to the ones used by Debuigne [7], and are presented in the next section.

3.2.1. Expression of the oxygen concentrations

The boundary conditions used in the calculation are illustrated in Fig. 3 and can be expressed by Eqs. (6)–(8):

$$\alpha_{Zr}: \begin{cases} C_\alpha = C_\alpha(0) & \text{for} \quad x = 0, t > 0 \\ C_\alpha = C_\alpha(\infty) & \text{for} \quad x > 0, t = 0 \end{cases} \tag{6}$$

$$\beta_{Zr}: \begin{cases} C_\beta = C_\beta(0) & \text{for} \quad x = 0, t > 0 \\ C_\beta = C_\beta(\infty) & \text{for} \quad x > 0, t = 0 \end{cases} \tag{7}$$

$$\phi: \begin{cases} C_\phi = C_{\phi/V} & \text{for} \quad x = x_0, t > 0 \\ C_\phi = C_{\phi/\alpha} & \text{for} \quad x = x_1, t > 0 \end{cases} \tag{8}$$

where $C_\alpha(\infty)$ is the oxygen concentration in α_{Zr} for $x = \infty$, in g/cm^3 and $C_\beta(\infty)$ is the initial oxygen concentration in β_{Zr}, in g/cm^3; x_0 is the position of the zirconia external surface

From Eq. (1) and the initial and boundary conditions, Eqs. (6)–(8), the oxygen concentrations in the different phases can be expressed

- In α_{Zr}:

From Eq. (6), oxygen concentration in α_{Zr} can be expressed as

$$C_\alpha = C_\alpha(0) - [C_\alpha(0) - C_\alpha(\infty)]\mathrm{erf}\left(\frac{x}{2\sqrt{D_\alpha t}}\right). \tag{9}$$

Like Debuigne [7], we assumed that $C_\alpha(\infty) = C_0$.

At the α/ϕ interface, we can get $C_\alpha = C_{\alpha/\phi}$ at $x = x_1$ and $t > 0$. So $C_\alpha(0)$ can be expressed as

$$C_\alpha(0) = \frac{C_{\alpha/\phi} - C_0\mathrm{erf}\left(\frac{x_1}{2\sqrt{D_\alpha t}}\right)}{1 - \mathrm{erf}\left(\frac{x_1}{2\sqrt{D_\alpha t}}\right)}. \tag{10}$$

Debuigne [7] rewrites Eq. (9) as follows:

$$\frac{C_\alpha - C_\alpha(\infty)}{C_\alpha(0) - C_\alpha(\infty)} = 1 - \mathrm{erf}\left(\frac{x}{2\sqrt{D_\alpha t}}\right). \tag{11}$$

Using the oxygen equilibrium concentration in the α_{Zr} phase at the α/ϕ and α/β interfaces, Eq. (11) can be expressed as

$$\frac{C_{\alpha/\phi} - C_\alpha(\infty)}{C_{\alpha/\beta} - C_\alpha(\infty)} = \frac{1 - \mathrm{erf}\left(\frac{x_1}{2\sqrt{D_\alpha t}}\right)}{1 - \mathrm{erf}\left(\frac{x_2}{2\sqrt{D_\alpha t}}\right)}. \tag{12}$$

From Eq. (12) we can get the oxygen diffusivity in the α_{Zr} phase.

- In β_{Zr}:

Using Eq. (7), oxygen concentration in β_{Zr} can be expressed as

$$C_\beta = C_\beta(0) + [C_\beta(0) - C_\beta(\infty)]\mathrm{erf}\left(\frac{x}{2\sqrt{D_\beta t}}\right). \tag{13}$$

For the β phase, $C_\beta(\infty) = C_0$.

At the β/α interface, we can get $C_\beta = C_{\beta/\alpha}$ at $x = x_2$ and $t > 0$. So $C_\beta(0)$ can be expressed as

$$C_\beta(0) = \frac{C_{\beta/\alpha} - C_0\mathrm{erf}\left(\frac{x_2}{2\sqrt{D_\beta t}}\right)}{1 - \mathrm{erf}\left(\frac{x_2}{2\sqrt{D_\beta t}}\right)}. \tag{14}$$

- In zirconia (ϕ):

The position of the zirconia external surface, x_0, can be written as

$$x_0 = x_1 - l_\phi. \tag{15}$$

Considering a parabolic kinetic regime for the zirconia growth (Wagner's theory), the zirconia layer thickness, l_ϕ, can be expressed as a function of time:

$$l_\phi = \sqrt{K_P^\phi t}. \tag{16}$$

where K_P^ϕ is the parabolic rate constant.

Moreover, the metal thickness consumed in oxidation, x_1, can be expressed as a function of l_ϕ using the Pilling–Bedworth ratio P ($P = 1.56$ for the Zr/ ZrO_2 system) which is the ratio of oxide volume grown to metal consumed. Also using Eq. (16), x_1 is expressed as

$$x_1 = \frac{l_\phi}{P} = \frac{\sqrt{K_P^\phi t}}{P}. \tag{17}$$

Finally, Eq. (15) becomes:

$$x_0 = \sqrt{K_P^\phi t}\left(\frac{1}{P} - 1\right). \tag{18}$$

Then, the solution of the diffusion equations can be written as

$$C_\phi = A + B\mathrm{erf}\left(\frac{x - x_0}{2\sqrt{D_\phi t}}\right). \tag{19}$$

Using Eq. (8), we can write:

$$\begin{cases} C_{\phi/V} = A \\ C_{\phi/\alpha} = A + B\mathrm{erf}\left(\frac{x_1 - x_0}{2\sqrt{D_\phi t}}\right) = A + B\mathrm{erf}\left[\frac{\frac{1}{P}\sqrt{K_P^\phi t} - \sqrt{K_P^\phi t}\left(\frac{1}{P} - 1\right)}{2\sqrt{D_\phi t}}\right] \\ \quad = A + B\mathrm{erf}\left(\dfrac{\sqrt{K_P^\phi}}{2\sqrt{D_\phi}}\right) \end{cases} \tag{20}$$

We can get

$$\begin{cases} A = C_{\phi/V} \\ B = \dfrac{C_{\phi/\alpha} - C_{\phi/V}}{\mathrm{erf}\left(\frac{\sqrt{K_P^\phi}}{2\sqrt{D_\phi}}\right)} \end{cases}. \tag{21}$$

Finally, the oxygen concentration in zirconia can be expressed as

$$C_\phi = C_{\phi/V} - \frac{(C_{\phi/V} - C_{\phi/\alpha})\mathrm{erf}\left[\frac{x + (P-1)x_1}{2\sqrt{D_\phi t}}\right]}{\mathrm{erf}\left(\frac{Px_1}{2\sqrt{D_\phi t}}\right)}. \tag{22}$$

3.2.2. The oxygen balance at the interface

The oxygen balance at the α/ϕ interface can be written as

$$\frac{dx_1}{dt} = \frac{-D_\phi\left(\frac{\partial C_\phi}{\partial x}\right)_{x=x_1} + D_\alpha\left(\frac{\partial C_\alpha}{\partial x}\right)_{x=x_1}}{PC_{\phi/\alpha} - C_{\alpha/\phi}}. \tag{23}$$

where dx_1/dt is the velocity of the α/ϕ interface relative to original surface, cm/s.

The Pilling–Bedworth ratio is used in order to accommodate the volume increase involved by the formation of the oxide from the alpha phase [4]. The evolution of x_1 as a function of time is given by Eq. (17).

The oxygen balance at the β/α interface can be written as

$$\frac{dx_2}{dt} = \frac{-D_\alpha\left(\frac{\partial C_\alpha}{\partial x}\right)_{x=x_2} + D_\beta\left(\frac{\partial C_\beta}{\partial x}\right)_{x=x_2}}{C_{\alpha/\beta} - C_{\beta/\alpha}}. \tag{24}$$

where dx_2/dt is the velocity of the α/β interface relative to the original surface, in cm/s.

Assuming that the growth of α_{Zr} from β_{Zr} follows a parabolic kinetic law, the position of the α/β interface x_2 can be expressed as follows:

$$x_2 = x_1 + l_\alpha = \frac{1}{P}\sqrt{K_p^\phi t} + \sqrt{K_p^\alpha t}. \tag{25}$$

where K_p^α is the parabolic rate constant for the growth of α_{Zr} from β_{Zr}, in cm^2/s.

3.2.3. Complementary data

In order to solve oxygen diffusivity from the equations derived above, it is necessary to have the experimental kinetic parameters (K_p^ϕ and K_p^α) and the equilibrium oxygen concentrations at the various interfaces.

Concerning the equilibrium oxygen concentration at the α/β interface, Chung and Kassner [10] investigated the zirconium-rich portion of the pseudobinary Zy-4/oxygen phase diagram. It is shown that the β phase boundary is virtually the same as that reported for the Zr–O system [12] while the α phase boundary is ~70 K lower than for the Zr–O system. For $T > 1280$ K, the phase boundaries between β and α phases can be represented as

$$\ln C_{\beta/\beta+\alpha} = 5.02 - 8220/T. \tag{26}$$

$$\ln C_{\alpha/\alpha+\beta} = -2.28 + 0.535\ln(T - 1083). \tag{27}$$

where $C_{\beta/\beta+\alpha}$ and $C_{\alpha/\alpha+\beta}$ are the oxygen concentration in wt% at respectively the β and α-phase boundaries at a given temperature T (Fig. 4).

For the ϕ/V and the α/ϕ interfaces, we use the oxygen concentrations calculated from the Zr–O binary system. The results are presented in Section 4.

The densities of Zy-4 and zirconia used in the calculations are 6.54 [8] and 5.82 [11] g/cm^3, respectively.

From experimental results recently determined in our laboratory [8], for low-tin Zy-4, K_p^ϕ and K_p^α can be expressed as

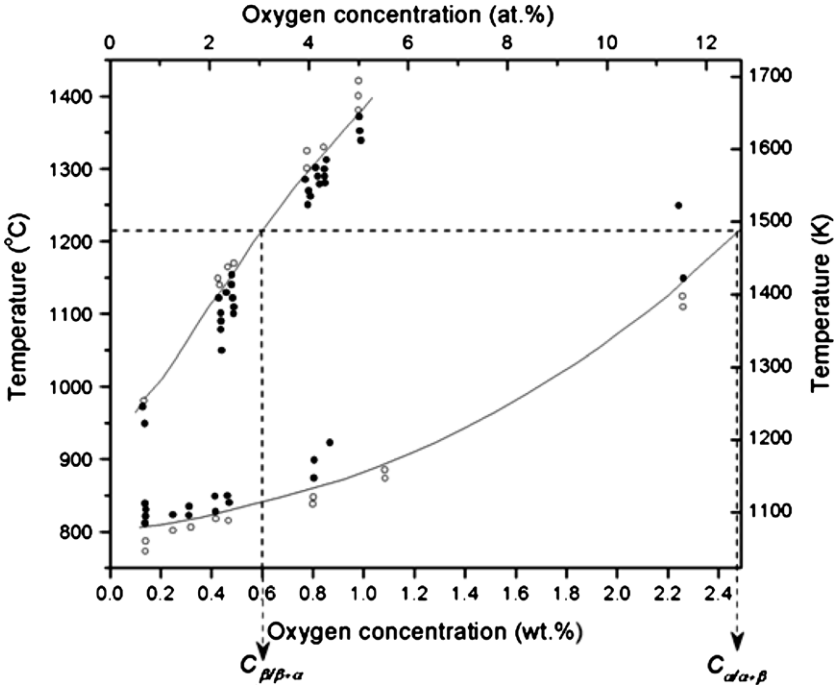

Fig. 4. α and β phase boundaries of the pseudobinary Zircaloy-4/oxygen phase diagram determined by metallographic analysis of equilibrated and quenched specimens by Chung et al. [4].

$$K_p^{\phi} = 9.2 \times 10^{-3} \exp\left(-\frac{1.406 \times 10^5}{RT}\right) \quad \text{in} \quad \text{cm}^2\ \text{s}^{-1}. \tag{28}$$

$$K_p^{\alpha} = 3.317 \times 10^{-1} \exp\left(-\frac{1.793 \times 10^5}{RT}\right) \quad \text{in} \quad \text{cm}^2\ \text{s}^{-1}. \tag{29}$$

4. Results and discussion

This paragraph aims at presenting the results obtained within this study. In a first step, the thermodynamic assessment of the binary Zr–O system was revised in order to take into account the existence of a non-stoichiometry for the 2 zirconia phases: α_{ZrO_2} and β_{ZrO_2}. This was necessary for the determination of the oxygen concentration at the metal/oxide interface ($C_{\phi/\alpha}$) for analytical diffusion modeling and for kinetic calculations using DICTRA software.

In a second step, the oxygen diffusion coefficients in ZrO_2, α_{Zr} and β_{Zr} were identified using an analytical model and our own experimental data which are

- ZrO_2 layer thickness
- Equilibrium oxygen concentrations at the ZrO_2/α and at α/β interfaces.

In a third step, we compared experimental and calculated oxygen concentration profiles. The experimental oxygen concentration profiles were obtained by EPMA from two methods:

(1) Partial dissolution of a pre-existing zirconia oxide layer at 973–1123 K.
(2) Different steam oxidation times in the temperature range 1273–1523 K.

4.1. Progress in the thermodynamic assessment of the Zr–O binary system

From the statement above, we know that in order to calculate the oxygen diffusivity, we need the equilibrium oxygen concentrations at the ϕ/V and α/ϕ interfaces. Since Zy-4 is a low-alloyed material, we can get these data by the thermodynamic calculation of the Zr–O binary system.

By metallographic observation [12,13] and by X-ray analysis [14], Domagala et al. [12] proved that the three different zirconia phases, α_{ZrO_2}, β_{ZrO_2} and γ_{ZrO_2}, are nonstoichiometric compounds. Until now, α_{ZrO_2} and β_{ZrO_2} were treated as stoichiometric compounds in the Zr–O binary system of Zircobase (version 04).

In the past few years, several groups contributed to the thermodynamic modelling of the Zr–O system due to its practical significance and the latest results are from Liang [15] and Wang [16]. In these studies, various thermodynamic models, especially for liquid, α_{Zr} and γ_{ZrO_2} phases, were used. But all of them treat α_{ZrO_2} and β_{ZrO_2} phases as stoichiometric compounds. In the present study, we take into account the composition range of α_{ZrO_2} and β_{ZrO_2}.

The Zr–O binary system is constituted by the following phases:

- Gas phase.
- The liquid solution phase.
- Terminal solid solutions: α_{Zr} phase, the solution of O in hcp Zr; β_{Zr} phase, the solution of O in bcc Zr.
- Zirconia: α_{ZrO_2} phase, the low-temperature phase with monoclinic structure; β_{ZrO_2} phase, the intermediate-temperature phase with tetragonal structure; γ_{ZrO_2} phase, the high-temperature cubic phase with CaF_2-type structure.
- ordered state of α_{Zr} phase at low-temperature: α'_{Zr}, Zr_6O, ZrO_x, Zr_6O_2 and ZrO_z.

In the thermodynamic database for zirconium alloys version 2004, Zircobase04 [1], the data from Liang et al. [15] were adopted. This set of data not only fit well with the experimental results, but also takes into account the ordered state of the α_{Zr} phase. In this work, based on the data in Zircobase04 [1], the Zr–O binary system was reassessed and the homogeneity ranges for α_{ZrO_2} and β_{ZrO_2} phases were taken into account.

4.1.1. Experimental and estimated data from the literature

The experimental phase diagram and thermodynamic data are summarized in Table 3 and the crystal structure data of ZrO_2 are listed in Table 4.

Kelley [17] measured the low-temperature heat capacities, in the temperature range 54.3–295 K, and he also calculated the entropy at 298 K, $S^{\circ}_{298\ K}$, using the Debye and Einstein function. Coughlin and King [18] obtained the heat capacities expression, Eq. (30), over the temperature range 298–1478 K using their measured enthalpy data.

$$C_p = 69.61 + 0.00753\,T - 1405588.9T^{-2} (\text{J mol}^{-1}\text{K}^{-1}). \tag{30}$$

The values from the two sources join smoothly at 298 K. But Coughlin and King [18] did not indicate the transition between α_{ZrO_2} and β_{ZrO_2} phases.

4.1.2. Thermodynamic models

A two-sublattice model $(Zr)_1(O,Va)_2$ was used, taking into account the non-stoichiometry of α_{ZrO_2} and β_{ZrO_2} (Va denotes vacancy). If ϕ denotes one of the phases, α_{ZrO_2} or β_{ZrO_2}, the Gibbs energy per mole of formula unit, G_m^{ϕ}, is given by

$$G_m^{\phi} = y_{Va}^{\circ} G_{Zr:Va}^{\phi} + y_O^{\circ} G_{Zr:O}^{\phi} + 2RT(y_{Va} \ln y_{Va} + y_O \ln y_O) + y_O y_{Va}[{}^0L_{Zr:O,Va}^{\varphi} + {}^1L_{Zr:O,Va}^{\varphi}(y_O - y_{Va}) + \ldots]. \tag{31}$$

Table 3
Experimental data for α_{ZrO_2} and β_{ZrO_2} phases

Type of data	Method	Value	Reference	
Lower limit of homogeneity range in α_{ZrO_2}	Metallography	–	[12]	+
Lower limit of homogeneity range in β_{ZrO_2}	Metallography	–	[12]	+
	Metallography	66.5 at.% O	[13]	–
	Metallography X-ray	64.7 at.% O, 1773 K	[14]	+
C_p for ZrO_2 (J mol^{-1} K^{-1})	Calorimetry		[17]	+
	Drop calorimeter		[18]	+
$S^{\circ}_{298\ K}$ for ZrO_2 (J mol^{-1} K^{-1})	Calculated using Debye and Einstein function	−194.37	[17]	+
$\Delta_f H^{\circ}_{298\ K}$ for ZrO_2 (kJ mol^{-1})	Combustion calorimetry	−1093.07 ±0.8	[19]	+
	Combustion calorimetry	−1099.75 ±2.1	[20]	+
	Calorimetry	−1079.276	[21]	+
	Calorimetry	−1081.784	[22]	+
	Calorimetry	−1070.498	[23]	+

The last column indicates that the data were used (+) or not used (−) in the present assessment.

Table 4
Crystal structure data for ZrO_2

Phase	Pearson symbol	Space group	Prototype	Reference
α_{ZrO_2}	*mP12*	$P2_1/c$	–	[24]
β_{ZrO_2}	*tP6*	$P4_2/nmc$	HgI_2	[24]
γ_{ZrO_2}	*cF12*	$Fm\bar{3}\,m$	CaF_2	[24]

where y_{Va} and y_O denote the site fractions of vacancy and oxygen respectively on the second sublattice. R is the gas constant, 8.314 J/(K mol) and T is the temperature, K. ${}^{\circ}G^{\phi}_{Zr:Va}$ represents the Gibbs energy of pure zirconium in phase $\phi(\phi = \gamma_{ZrO_2}\beta_{ZrO_2})$, or ${}^{\circ}G^{\phi}_{Zr:O}$ the Gibbs energy of the stoichiometric zirconia, which has the same expression as for pure element [25]:

$$ {}^{\circ}G^{\phi}_{Zr:O}(T) = a + bT + cT\ln T + dT^2 + eT^{-1}. \quad (32) $$

The ${}^{i}L^{\phi}_{Zr:O,Va}$ $(i = 0,1,\ldots)$ represents the interaction parameters between the O and Va elements in the second sublattice with the first sublattice occupied by Zr.

4.1.3. Thermodynamic optimization

The optimization started with the stoichiometric ZrO_2. The heat capacity from Coughlin and King [18] was adopted, and it was assumed that α_{ZrO_2} and β_{ZrO_2} have the same expression, Eq. (30). Corresponding to the expression of the Gibbs energy of stoichiometric compound in Eq. (32), the heat capacity can be described with the following expression:

$$ C_p = -c - 2dT - 2eT^{-2}. \quad (33) $$

Compared with Eq. (30), the parameters from c to e in Eq. (32) can be derived directly.

Then the standard heat of formation, $\Delta_f H^{\circ}_{298\ K}$ [19–23] and entropy, $S^{\circ}_{298\ K}$ [17] for ZrO_2 were used to determine the initial values of a and b in Eq. (32) for stoichiometric compound α_{ZrO_2} and β_{ZrO_2}.

At the end, the experimental data on phase equilibria [12–14] were taken into the assessment.

The thermodynamic description and the invariant reactions related to α_{ZrO_2} and β_{ZrO_2} phases obtained in the present assessment are listed in Tables 5 and 6, respectively.

Fig. 5(a) shows the comparison of the calculated phase diagram with the experimental data with critical temperature labeled. But the ordered state of α_{Zr} phase at low-temperature is excluded. Fig. 5(b) represents a blow-up of the $\alpha_{ZrO_2}/\beta_{ZrO_2}$ region.

Table 5
Optimized thermodynamic parameters of α_{ZrO_2} and β_{ZrO_2} phases

Phase	Model	Parameter (J/mol)
α_{ZrO_2}	Zr_1 (O, Va)$_2$	${}^{\circ}G^{\alpha ZrO_2}_{Zr:O} = -1129350.1 + 428.7287\,T - 69.5552T\ln(T) - 0.003762T^2 + 702240T^{-1}$
		${}^{\circ}G^{\alpha ZrO_2}_{Zr:Va} = 9852.885 + 23.4345T + {}^{\circ}G^{hcp}_{Zr}$
β_{ZrO_2}	Zr_1 (O, Va)$_2$	${}^{\circ}G^{\beta ZrO_2}_{Zr:O} = -1110998.003 + 416.3114T - 69.5552T\ln(T) - 0.003762T^2 + 702240T^{-1}$
		${}^{\circ}G^{\beta ZrO_2}_{Zr:Va} = 9852.885 + 23.4345T + {}^{\circ}G^{hcp}_{Zr}$

Fig. 6 presents the comparison between the computed results (solid lines) and the experimental data for the heat of formation $\Delta_f H^{\circ}_{298\ K}$ and the entropy $S^{\circ}_{298\ K}$ for stoichiometric α_{ZrO_2}.

It is shown that the reassessed results fit well with the data from the literature. It is drawn from the discussion above that a consistent set of thermodynamic data for zirconia was obtained after the optimization by means of CALPHAD methodology. From the assessed parameters, we evaluate the corresponding parameters in Zircobase04 [1] and name the revised thermodynamic database as Zircobase06.

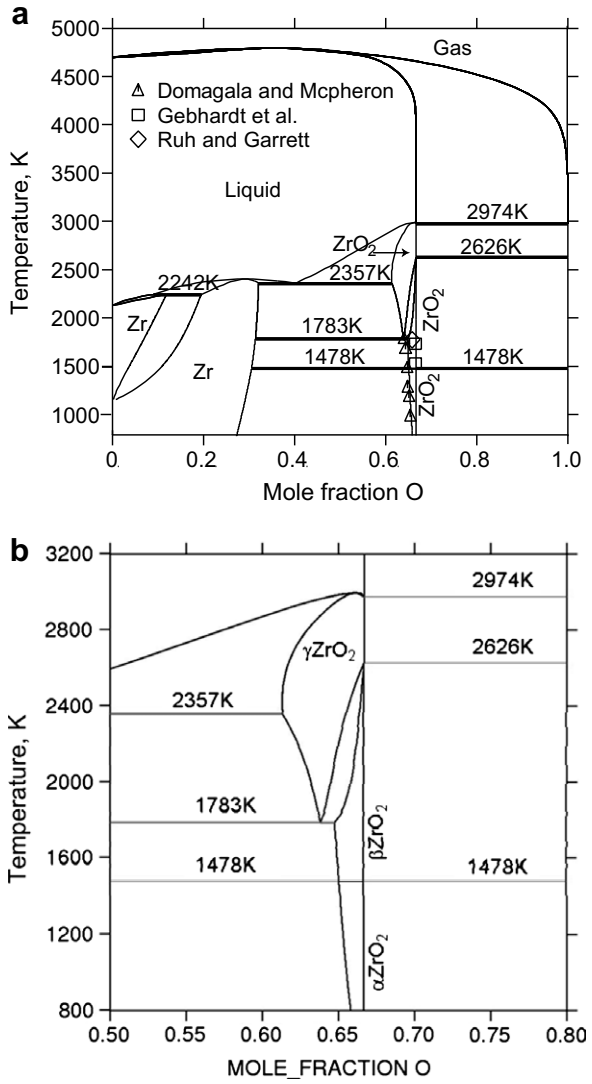

Fig. 5. (a) Zr–O phase diagram, calculated by the present thermodynamic description compared with the experimental measurements [12–14]. (b) Blow-up of the Zr–O calculated phase diagram showing the ZrO_2 region.

Table 6
Invariant reactions related to α_{ZrO_2} and β_{ZrO_2} phases

Reaction	Liang and Lukas [15]				Present work			
	T (K)		x(O)		T (K)		x(O)	
$\alpha_{ZrO_2} \leftrightarrow \alpha_{ZrO_2} + ZrO_2$	722	0.2693	–	0.3037	722	0.2692	0.6592	0.3036
$\beta_{ZrO_2} \leftrightarrow \alpha_{Zr} + \alpha_{ZrO_2}$	1478	–	0.3037	–	1478	0.6505	0.3053	0.6505
$\beta_{ZrO_2} \leftrightarrow$ Gas $+ \alpha_{ZrO_2}$	1478	–	1.0000	–	1478	0.6667	1.0000	0.6667
$\gamma_{ZrO_2} \leftrightarrow \alpha_{Zr} + \beta_{ZrO_2}$	1783	0.6385	0.3136	–	1783	0.6385	0.3136	0.6476
$\gamma_{ZrO_2} \leftrightarrow$ Gas $+ \beta_{ZrO_2}$	2626	–	1.0000	–	2626	0.6667	1.0000	0.6667

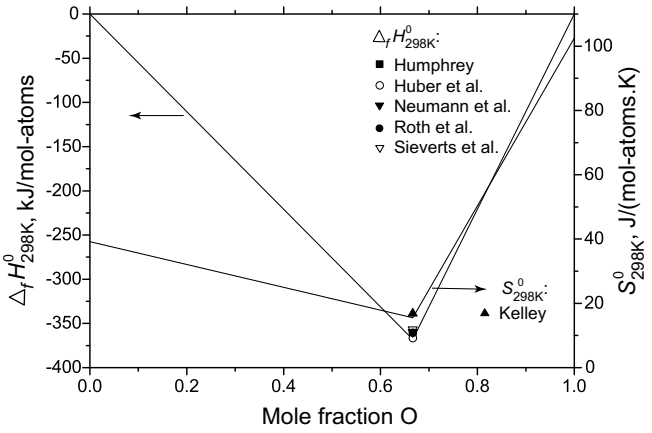

Fig. 6. Calculated enthalpy of formation and entropy at 298 K compared with the experimental data [19–23] for α_{ZrO_2}.

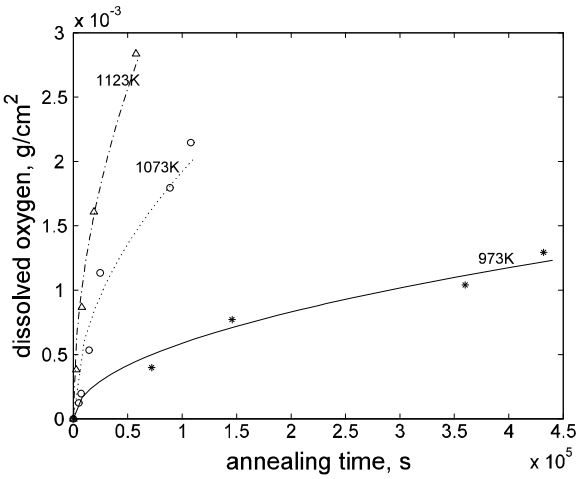

Fig. 8. Variation of the amount of dissolved oxygen with time at three different temperatures, 973 K, 1073 K and 1123 K.

4.2. Oxygen diffusivity in α_{Zr} of Zy-4 at intermediate-temperatures (upper α temperature range)

4.2.1. Identification of the oxygen diffusion coefficient in α_{Zr}

Fig. 7 represents the SEM micrographs of sample B before and after heat treatment at 1073 K for 4 h.

The oxide film thickness and oxygen diffusion coefficient in α_{Zr} phase of low-tin Zy-4 at different temperatures are listed in Table 7. l_ϕ is the thickness of zirconia layer after each heat treatment and $l_{\phi,0} - l_\phi$ is the thickness of zirconia dissolved during the heat treatment. The amount of oxygen dissolved during the heat treatment, M, is calculated from these data, following the method described in Section 3.1. The variation of the amount of dissolved oxygen with time at various temperatures is plotted in Fig. 8 and the linear

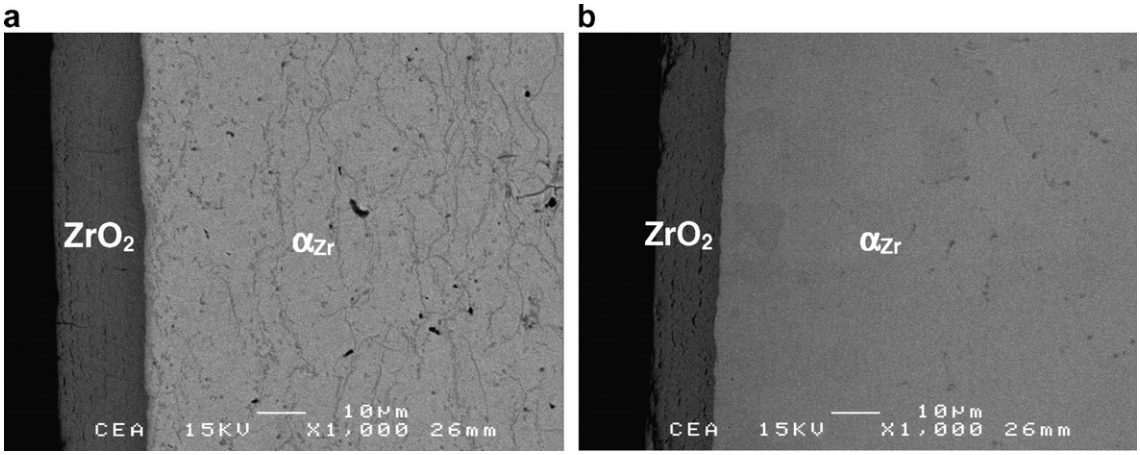

Fig. 7. SEM micrograph of specimen B before (a) and after (b) heat treatment at 1073 K for 4 h.

Table 7
Oxide film thickness and oxygen diffusion coefficients in α_{Zr} phase at different temperatures

Temperature, K	Phases	Time	l_ϕ, μm	$l_{\phi,0} - l_\phi$, μm	Sample	D, cm^2/s
973	α_{Zr}	20 h	20.0 ± 1.9	2.6	A	1.918×10^{-11}
		40 h 30 min	11.7 ± 3.0	5.1	B	
		100 h	15.8 ± 3.7	6.8	A	
		120 h	8.2 ± 2.5	8.6	B	
1073	α_{Zr}	1 h25 min	16.0 ± 1.8	0.8	B	1.984×10^{-10}
		2 h	21.4 ± 3.8	1.2	A	
		4 h	13.3 ± 1.0	3.5	B	
		6 h50 min	15.1 ± 3.6	7.5	A	
		24 h40 min	10.8 ± 3.3	11.8	A	
		30 h	8.5 ± 2.4	14.1	A	
1123	α_{Zr} (+β_{Zr})[a]	45 min	20.1 ± 3.4	2.5	A	6.957×10^{-10}
		2h10 min	16.9 ± 3.0	5.7	A	
		5h15 min	12.0 ± 3.6	10.6	A	
		16 h	3.9 ± 2.2	18.7	A	

[a] Equilibrium fraction of $\beta_{Zr} \sim 20\%$.

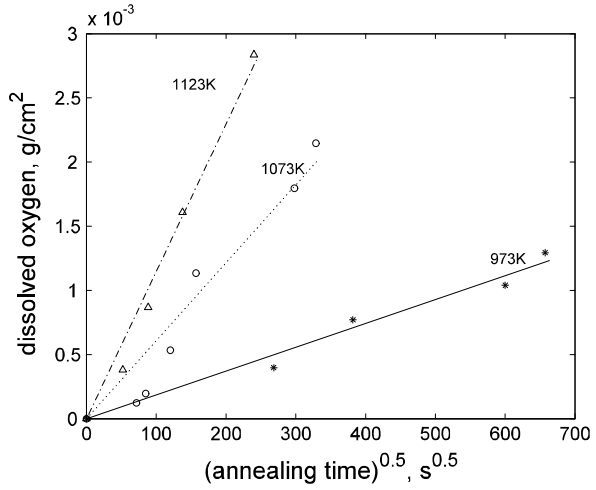

Fig. 9. The linear relation of the amount of oxygen dissolved from zirconia into α_{Zr} as a function of time$^{1/2}$ at three different temperatures, 973 K, 1073 K and 1123 K.

relationship between the amount of oxygen dissolved from the oxide film into the α_{Zr} phase and (annealing time)$^{0.5}$ at various temperatures is shown in Fig. 9. The linear fits of the data reported in Fig. 9 are used to calculate the oxygen diffusion coefficients, D_α, following Eq. (5). The D_α values are then reported on a Arrhenius plot (Fig. 10) which allows to obtain the following expression of the oxygen diffusion coefficient in α_{Zr}:

$D_\alpha = 6.798\exp(-21799\text{kJ}/RT)\ \text{cm}^2/\text{s}$. (in the 973–1123 K temperature range which corresponds to a α and $\alpha + \beta$ temperature range).

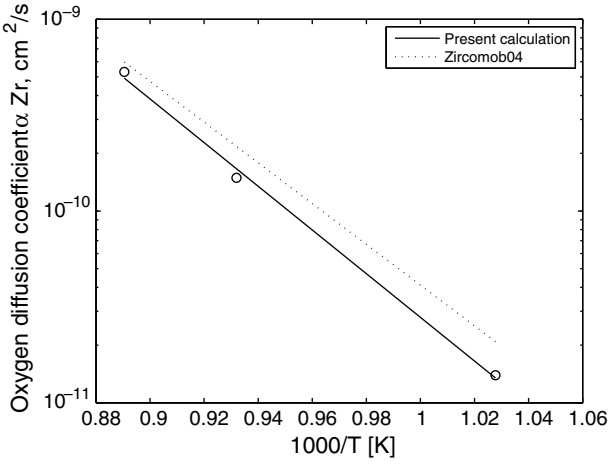

Fig. 10. Comparison of oxygen diffusion coefficient in α_{Zr} of Zy-4 obtained from this work and in α_{Zr} of pure zirconium taken from Zircomob04 [2].

4.2.2. Comparison of calculated and experimental results

From the calculated oxygen diffusivity D_α, the concentration profiles at different times and temperatures were computed (Fig. 11). It is shown that the calculated concentration profiles fit well with our experimental results.

It is shown in Fig. 10 that, at low-temperature, oxygen diffusion coefficient in α_{Zr} phase of low-tin Zy-4 is quite similar to the oxygen diffusivity in α_{Zr} phase of pure zirconium.

4.3. Oxygen diffusivity at high temperature (β_{Zr} temperature range)

4.3.1. Identification of the oxygen diffusion coefficient in α_{Zr}, β_{Zr} and ZrO_2

In Eqs. (16) and (18) there are three unknown parameters D_α, D_β and D_ϕ. From Eq. (12), we can get the oxygen diffusivity in α_{Zr} of Zy-4 and then combining Eqs. (23) and (24) and the related parameters in the equations, the oxygen diffusivity in β_{Zr} and zirconia phases can be determined.

The calculated oxygen diffusivities are shown in Table 8 and Fig. 12. As a comparison we also give the results from the literature [2,4,5,26].

For α_{Zr} and β_{Zr}, it is shown in Table 8 and Fig. 12 that the calculated oxygen diffusivities fit well with the values from the

Table 8
Comparison of the oxygen diffusivities

		D_0, cm^2/s	Q, kJ/mol
α_{Zr}	Present calculation	1.543	201.55
	Pawel [4]	3.920	213.18
	Zircomob04 [2]	1.710	203.29
β_{Zr}	Present calculation	0.0068	102.62
	Perkins [5]	0.0248	117.88
	Zircomob04 [2]	0.0202	115.17
ZrO_2	Present calculation	0.116	143.64
	Oberländer [26]	0.140	1.40
	Pawel [4]	0.127	1.442
	Zircomob04 [2]	0.00105	1.226

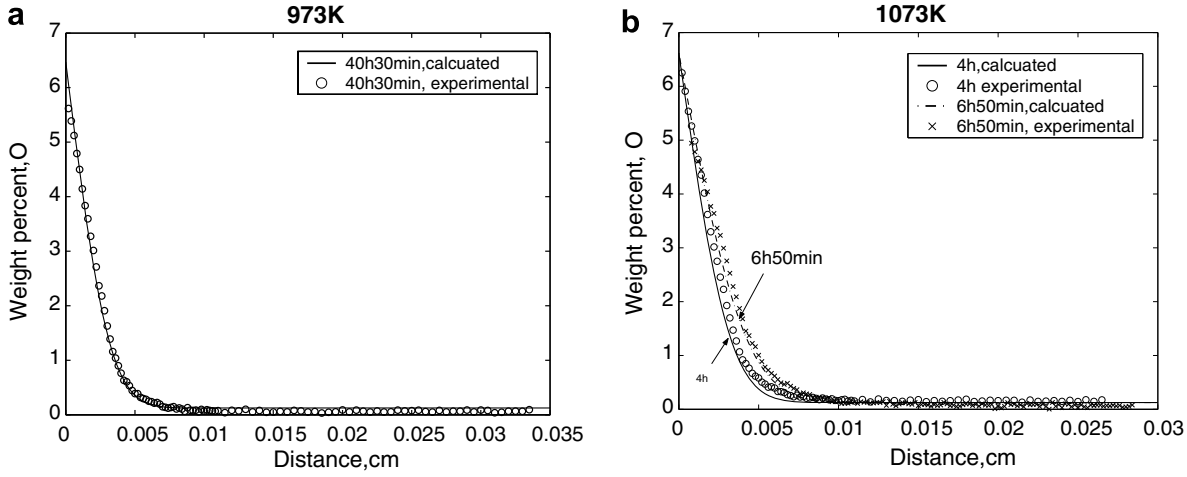

Fig. 11. Comparison of the experimental and calculated concentration profiles in α_{Zr} at 973 K (a) and 1073 K (b).

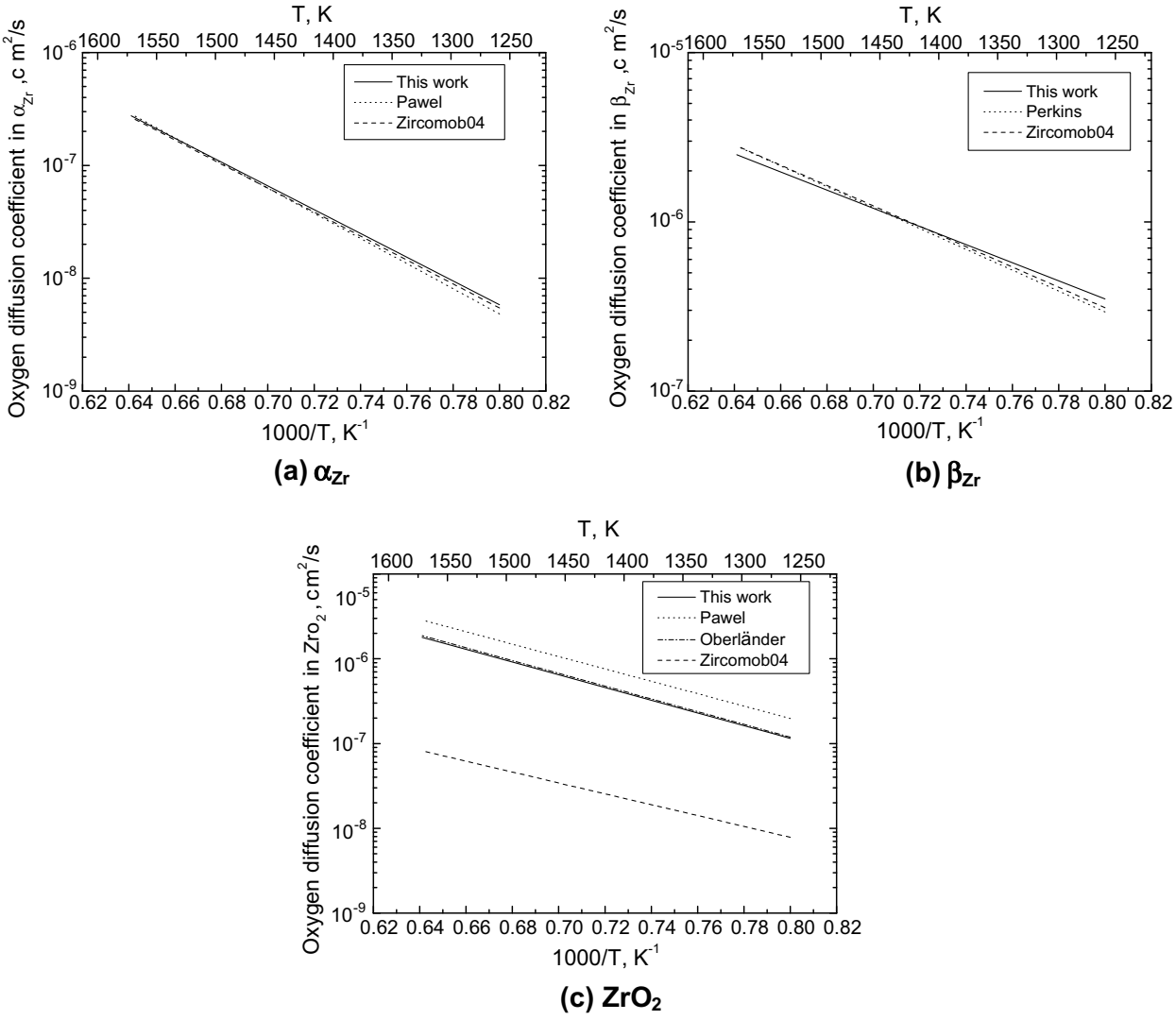

Fig. 12. Comparison of the oxygen diffusivities between present calculation at 1273–1523 K and the values from literatures [2,4,5,26] (a) α_{Zr}, (b) β_{Zr}, (c) zirconia.

literature [2,4,5,26]. For zirconia, the calculated results fit well with the results from Pawel [4] but are much different from the value from Zircomob04 [2]. The possible reason for this is that in Zircomob04 [2] the temperature range of oxygen diffusivity [2] in ZrO_2 corresponds to lower temperatures, 650–1100 K.

At last, taking into account the results obtained at Section 4.2.1, all the data obtained for D_α in the whole temperature range have been plotted against 1000/T to finally obtain the following diffusion coefficient of oxygen in α_{Zr} for 973 K $\langle T <$ 1523 K: $D = 4.604 \exp(-214.44\ \text{kJ}/RT)\ \text{cm}^2/\text{s}$ (Fig. 13).

4.3.2. Comparison of calculated and experimental results

By the calculated oxygen diffusivities and the related experimental parameters and by the concentration expression in the phases, Eqs. (9)–(13), (14), (20)–(22), we can calculate the concentration profiles. Fig. 14 shows the comparison of concentration profiles between calculated results and experimental data [8] at 1473 K.

From Fig. 14, it is shown that for short time diffusion, for example 55 s and 187 s, the calculated results fit well with experimental results. But in the enlarged part of β_{Zr}, it is shown that for long time diffusion, for example 520 s and 1429 s, the calculated results give lower concentration values than the experimental data. This is due to the fact that this model [7] is used for a semi-infinite system. In our case, within the limited time of the experiments, β_{Zr} phase side

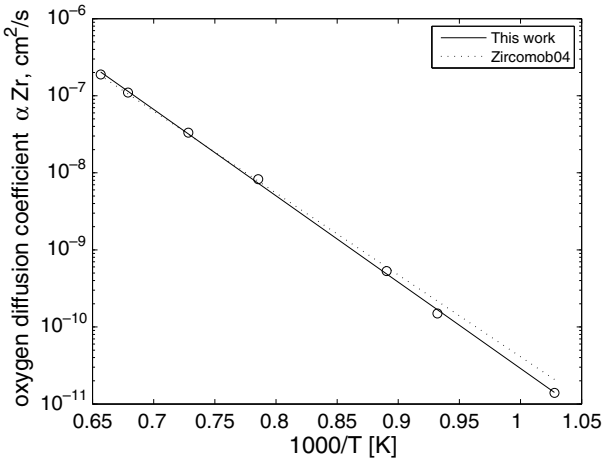

Fig. 13. Oxygen diffusion coefficient in α_{Zr} of Zy-4 against 1000/T in the temperature range 973 K $\langle T \rangle$ 1523 K.

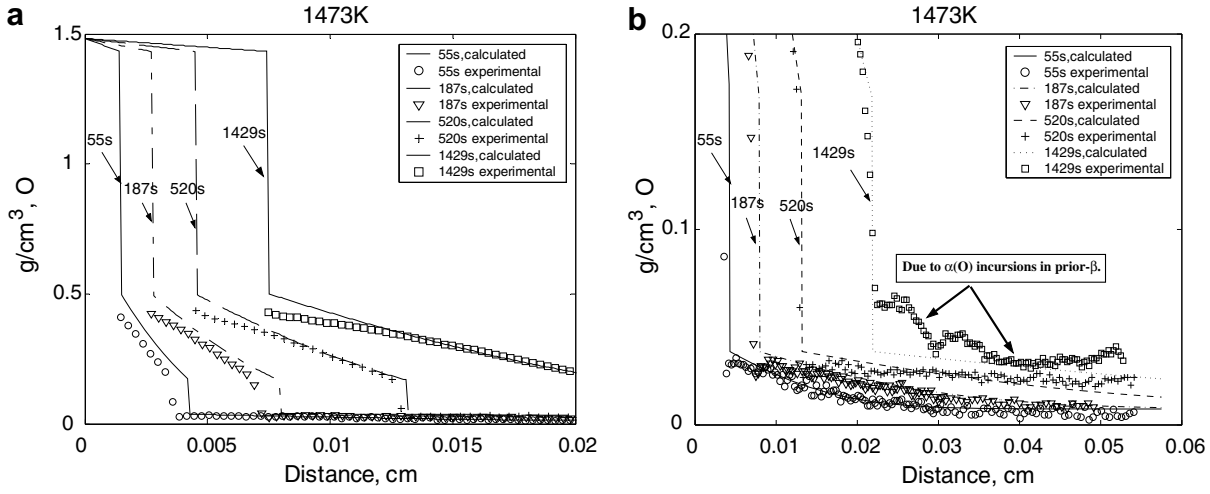

Fig. 14. Comparison of the calculated and experimental concentration profiles at 1473 K, (b) enlarged part of β_{Zr} phase in (a).

has been treated as semi-infinite. But in reality, the system has to be considered as finite (the thickness of the wall cladding tube is closed to ~600 μm). The experimental oxygen concentrations in β_{Zr} are thus higher than the calculated results due to the finite thickness of the sample (i.e., no oxygen flux at $x \sim 600$ μm).

5. Conclusion

In this work, oxygen diffusion coefficients in low-tin Zy-4 alloy were determined by an 'inverse' method for:

- α_{Zr} in the temperature ranges 973–1123 K and 1373-1523 K;
- β_{Zr} in the temperature range 1373–1523 K;
- and ZrO_2 in the temperature range 1373–1523 K.

These determinations were performed using analytical models.

Different kinds of data were necessary to apply these models, thus experiments were performed in order to determine the thickness of the zirconia layer as a function of time and temperature.

It was also necessary to determine the oxygen concentration at the different phase interfaces; the thermodynamic description of the binary Zr–O system was improved in order to take into account the nonstoichiometry of α_{ZrO_2} and β_{ZrO_2} as it was experimentally shown by different authors.

It appears that the calculated oxygen diffusivity in α_{Zr} phase of low-tin Zy-4 alloys at temperatures below and above the α/β transition, have similar values. By comparing with the data from the kinetic database for Zr alloys (version 2004), Zircomob04, it was shown that the oxygen diffusivity in α_{Zr} and β_{Zr} phases of low-tin Zy-4 alloys are quite similar to the ones in α_{Zr} and β_{Zr} of pure zirconium.

However, for the oxide phase (zirconia), the calculated results for low-tin Zy-4 are different from the value obtained with pure zirconium. By comparing the calculated and the experimental oxygen concentration profiles in β_{Zr}, it is shown that the analytical model from Debuigne's thesis [7] can only be used for short oxidation times. For longer oxidation times, it would be necessary to take into account the finite dimensions of the sample.

Acknowledgement

The authors are thankful to AREVA-NP (J.P. Mardon) for supplying materials.

References

[1] N. Dupin, I. Ansara, C. Servant, C. Toffolon, C. Lemaignan, J.C. Brachet, J. Nucl. Mater. 275 (1999) 287.
[2] C. Toffolon-Masclet, M. Mathon, A. Engström, J.C. Brachet, Poster presentation at the 14th International Symposium on Zirconium in the Nuclear Industry, June 13–17 2004, Stockholm, Sweden.
[3] J.O. Andersson, T. Helander, L.H. Hoglund, P.F. Shi, B. Sundman, CALPHAD 26 (2002) 273.
[4] R.E. Pawel, J. Electrochem. Soc. 126 (1979) 1111.
[5] R.A. Perkins, J. Nucl. Mater. 68 (1977) 148.
[6] C.J. Rosa, W.C. Hagel, Trans. Metall. Soc. AIME 242 (1968) 1293.
[7] J. Debuigne, Study of the zirconium oxidation and the oxygen diffusion in oxide and metal. PhD thesis, Paris University, 1966, in French.
[8] J.C. Brachet, V. Vandenberghe et al., Hydrogen Content, Pre Oxidation and Cooling Scenario Influences on Post-Quench Mechanical Properties of Zy-4 and M5(R) alloys in LOCA conditions - Relationship with the post-Quench Microstructure, ASTM 15th International Symposium on Zirconium in the Nuclear Industry, June 24–28 2007, Sunriver, Oregon.
[9] U. Roy, Acta Metall. 16 (1968) 243.
[10] H.M. Chung, T.F. Kassner, J. Nucl. Mater. 84 (1979) 327.
[11] J.D.H. Donnay (Ed.), ACA Monograph, vol. 5, American Crystallographic Association, USA, 1963, p. 142.
[12] R.F. Domagala, D.J. McPherson, Trans. AIME 200 (1954) 238.
[13] E. Gebhardt, H.D. Seghezzi, Würrschnabel, J. Nucl. Mater. 4 (1961) 255. In German.
[14] R. Ruh, H.J. Garrett, J. Am. Ceram. Soc. 50 (1967) 257.
[15] P. Liang, N. Dupin, S.G. Fries, H.J. Seifert, I. Ansara, H.L. Lukas, F. Aldinger, Z. Metallkd. 92 (2001) 747.
[16] C. Wang, M. Zinkevich, F. Aldinger, CALPHAD 28 (2004) 281.
[17] K.K. Kelley, Ind. Eng. Chem. 36 (1944) 377.
[18] J.P. Coughlin, E.G. King, J. Am. Chem. Soc. 72 (1950) 2262.
[19] G.L. Humphrey, J. Am. Chem. Soc. 76 (1954) 978.
[20] Elmer J. Huber Jr., Earl L. Head, Charles E. Holley Jr., J. Phys. Chem. 68 (1964) 3040.
[21] B. Neumann, C. Kröger, H. Kunz, Z. Inorg. Chem. 218 (1934) 379. In German.
[22] W.A. Roth, E. Borger, H. Siemonsen, Z. Anorg. Chem. 239 (1938) 321. In German.
[23] A. Sieverts, A. Gotta, S.Z. Halberstadt, Anorg. Chem. 187 (1930) 155. In German.
[24] ASM Handbook volume 3 Alloy phase diagrams, in: H. Baker (Ed.), ASM International, Materials Park, OH, 1992, Section 2, 326.
[25] A.T. Dinsdale, Calphad 15 (1991) 317.
[26] B. Oberländer, P. Kofstad, I. Kvernes, Mat.–wiss. U. Werkstoffech. 19 (1988) 190.